Nd-Fe-Al, A SPIN GLASS TRANSITION IN A COLLECTION OF SUPERPARAMAGNETIC CLUSTERS

R. W. McCALLUM[1,2], M. J. KRAMER[1,2], K. W. DENNIS[1]

[1]*Metal & Ceramic Sciences Program, Ames Laboratory (USDOE) and*
[2]*Materials Science and Engineering Department*
Iowa State University, Ames, IA, 50011, USA

L. H. LEWIS

Materials Science Department,
Brookhaven National Laboratory, Upton, New York 11973-5000

In the Nd-Fe-Al system, compositions in the range of $Nd_{60}Fe_{30}Al_{10}$ have been reported to be ferromagnetic bulk metallic glasses with high coercivities. Careful examination of both the microstructure and magnetic properties of these materials shows this to be true only in the most general sense. The materials are shown to be nanocomposites, in the strictest sense, with characteristic structural length scales on the order of 1.2 nm. Magnetically, the materials are also composites exhibiting a number of magnetic transitions as a function of temperature. The temperature dependence of the magnetic properties will be discussed in terms of strongly-interacting superparamagnetic clusters residing in a paramagnetic matrix. The clusters exhibit a frequency-dependent blocking temperature as determined from AC susceptibility, that is is inconsistent with simple superparamagnetic behavior but is consistent with a spin glass-type ordering of the clusters to form a cluster glass. For a temperature region extending approximately 100 K below the cluster glass ordering temperature, the materials exhibit low coercivity. Below this temperature regime significant coercivities develop. The energy barrier to magnetic reversal provided by the product of the cluster volume multiplied by the anisotropy energy is inconsistent with the values required to fit the superparamagnetic behavior above the spin glass transition in the framework of the random anisotropy model. Instead, the existence in this system of significant coercivity is associated with a change in the paramagnetic fraction of the sample consistent with antiferromagnetic ordering of part of the paramagnetic matrix. The remainder of the matrix material orders ferromagnetically at a lower temperature and the interaction between the antiferromagnetic clusters and the ferromagnetic matrix underlies the large coercivities observed at low temperatures.

1. Introduction

In 1996 Inoue and co-workers announced[1], the development of amorphous ferromagnetic (Bulk Metallic Glass) BMG alloy rods of 1 – 12 mm in diameter that possessed appreciable coercivities at room temperature. Since that time, $RE_{60}Fe_{30}Al_{10}$ (RE=Nd or Pr) and related alloys modified by Co[2] and Ce and Si[3] have generated considerable interest of both applied and fundamental nature because of the magnitude of this reported coercivity, up to 0.4 T at room temperature. Coercivity in amorphous ferromagnets has traditionally been understood in terms of the random anisotropy model[4]. This model incorporates weak interparticle interactions into the Stoner-Wohlfarth[5] model and relies on single-particle anisotropy to provide the barrier to magnetization reversal. As a result, the barrier height is given by the product Kv of the volume of the particle, v, and the magnetocrystalline anisotopy constant, K. The random anisotropy model has been extended to include the role of thermal fluctuations in reducing the effective barrier height and thus the temperature dependence of the coercivity may be used to determine the barrier height to magnetic reversal[6]. This model provides qualitative agreement with the experimentally determined temperature dependence of a number of amorphous systems; however the Kv product required to fit the data requires either a cluster volume inconsistent with the structural data or an anistropy energy which is much larger than corresponding bulk values. To explain the room temperature

coercivity of $RE_{60}Fe_{30}Al_{10}$ in terms of the random anisotropy model, the Kv product must be 1 - 2 orders of magnitude larger than that observed in other systems. In order to clarify the origin of the coercivity in the reported BMG alloys $R_{60}Fe_{30}Al_{10}$ (R = Nd or Pr) as well as to assess their promise as novel permanent magnets, a comprehensive structural and magnetic study of amorphous melt-spun samples of nominal composition $Nd_{60}Fe_{30-x}Al_{10+x}$ ($-2 \leq x \leq 6.5$) was undertaken. It is expected that the solidification route, microstructure, and composition of melt-spun ribbons of this composition are more homogeneous than those of their bulk analogues. Insight into the structure-magnetic property relationships inherent to this family of alloys gained from studies on melt-spun ribbons can be applied to studies on bulk cast forms of these materials.

As reported in part by the present authors elsewhere[7,8], solidification from the melt of the alloy $Nd_{60}Fe_{30}Al_{10}$ does not result in an entirely amorphous material; rather, highly-stable nanoscopic aluminide and/or silicide phases, or motes, are found to be present in the melt prior to solidification of melt-spun, nominally-amorphous alloys of $Nd_{60}Fe_{30}Al_{10}$. Not only do these motes affect the short-range order of the system and provide heterogeneous nucleation sites for crystallization, they also determine the magnetic properties of the alloy. It is found that the coercivity of the resultant largely-amorphous materials arises from magnetic exchange coupling between the ferromagnetic (F) matrix and the antiferromagnetic (AF) motes, which results in a very strong interaction analogous to the "exchange-bias" coupling found in F-AF nanosystems. Furthermore, the counterintuitive empirical observation[9] that cast rods of the purported BMG compositions possess an amorphous interior and a nanocrystalline exterior may be explained on the basis of solidification in the pertinent region of the Nd-Fe-Al ternary phase diagram. This explanation provides a scientific underpinning to the often-reported confusing empirical observation of signficiant differences in the magnetic behavior of cast rods and melt-spun ribbons of the $Nd_{60}Fe_{30}Al_{10}$ composition.

2. Sample preparation

All samples were made from high purity Nd (99.95%), Fe (99.99%) and Al (99.999%). Initial ingots were arc-melted under high-purity Ar. To synthesize ingots for melt spinning, the Nd and Fe were arc-melted together and then the Al was subsequently added as this route has been found to reduce the formation of refractory phases during intial melting[14]. If these refractory phases do form in the initial melt, there may not be sufficient time for them to dissolve during subsequent melting steps. The ingots were induction-melted in a quartz crucible at 1000 °C and then melt-spun onto a copper wheel with a tangential surface speed of 25 m/s in 1/3 atmosphere of helium. Solidification of the melt-spun alloy proceeded from the contact surface of the ribbon to the copper wheel (the "wheel side") through the ribbon to the ribbon surface in contact with the helium atmosphere (the "free side"). Five nominal ribbon compositions, which cross the (Nd - δ-phase) two-phase region in the equilibrium Nd-Fe-Al phase diagram[10] as shown in Fig. 1, were investigated. The compositions were $Nd_{61}Fe_{31}Al_8$, $Nd_{60}Fe_{30}Al_{10}$, $Nd_{59}Fe_{29}Al_{12}$, $Nd_{60}Fe_{26}Al_{14}$ and $Nd_{60}Fe_{23.6}Al_{16.4}$.

3. Characterization of Microstructure

The details of the microstructural characterization including X-ray diffraction (XRD) using both high energy and Cu-K_α radiation as well as Transmission Electron Microscopy (TEM) have

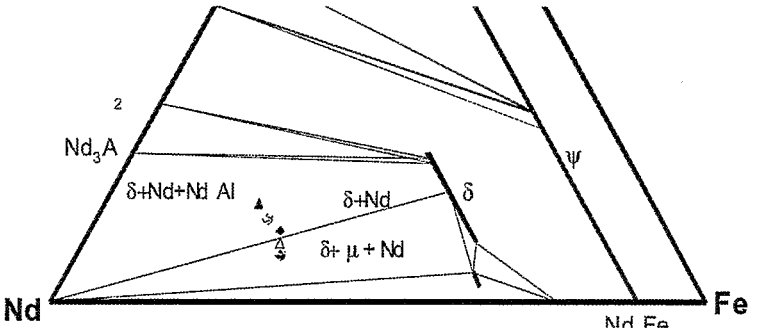

Figure 1: Partial view of the Nd-Fe-Al phase diagram. The equilibrium ternary phases are $\delta = Nd_6Fe_{14-x}Al_x$ ($2<x<5.5$), $\mu = Nd_{33.3}Fe_{64.2-x}Al_{2.5+x}$ ($2.5<x<5$), and $\psi = Nd_2Fe_{17-x}Al_x$ ($0<x<7$). The compositions of the amorphous ribbon samples are $Nd_{61}Fe_{31}Al_8$ (●), $Nd_{60}Fe_{30}Al_{10}$ (⮟), $Nd_{59}Fe_{29}Al_{12}$ (◆), $Nd_{60}Fe_{26}Al_{14}$ (○), and $Nd_{60}Fe_{23.6}Al_{16.4}$ (▲).

previously been reported. While the ribbons appear amorphous using XRD and Selected Area Diffraction (SAD) patterns in the TEM, Conical Dark Field (CDF) TEM images revealed that the melt spun ribbons contain as high density of clusters with 1-2 nm average size.

A Lakeshore Vibrating Sample Magnetometer (VSM) equipped with a 2.2 T magnet was used to measure the magnetization response of the samples versus temperature in the range 300 K $< T <$ 1200 K. By virtue of their high rare-earth content the samples have a strong tendency to oxidize; therefore they were sealed in quartz capillary ampoules in an inert atmosphere. A paramagnetic La sphere was placed in the ampoule to getter oxygen. The La sphere was separated from the sample by a piece of quartz rod. After the ampoule sealed, the La was heated in a small tube furnace to 700°C while the sample was held at room temperature. This process removed all residual O_2 prior to measurement. Quantum Design MPMS SQUID magnetometers were used to measure AC and DC magnetization in the temperature range from 2 K to 400 K. The melt-spun ribbons were mounted parallel to the field direction and no correction for demagnetization was made. Measurements made below room temperature were taken both in the zero-field-cooled (ZFC) and field-cooled (FC) modes in order to characterize the onset of irreversible magnetic character. Magnetization (M) *vs.* field (H) curves from 5T to –5T were measured in decreasing fields after field-cooling the sample in a 5 T field from 400 K to the measurement temperature. In addition thermoremanent magnetization curves were obtained by cooling the sample from 400 K to 5 K in a 0.1 T field, setting the field to zero and measuring the remanent magnetization as a function of temperature. AC measurements were performed at 0.1, 1.0, 10, 100, and 1000 Hz to measure the time dependent properties of the sample. The AC amplitude was 0.2 mT with no DC bias field.

4. Results

The initial magnetic characterization was performed using DC magnetization over the temperature range from 2 K to 880 K. Ribbons of all five compositions were characterized and the data for $Nd_{60}Fe_{30}Al_{10}$ are presented in Figure 2. This figure combines ZFC and FC SQUID magnetization measurements with VSM data collected on warming from room temperature. The measurement field was 0.1 T. The DC data exhibits three distinct features: an apparent ferromagnetic transition at T = 600 K, a divergence of the ZFC and FC curves at T = 280 K and an increase in the magnetization with decreasing temperature below T =50 K. The temperatures at which these features occur vary with composition in a systematic fashion that will be discussed later. M *vs.* H measurements were performed for a number of temperatures below 400 K and present an equally

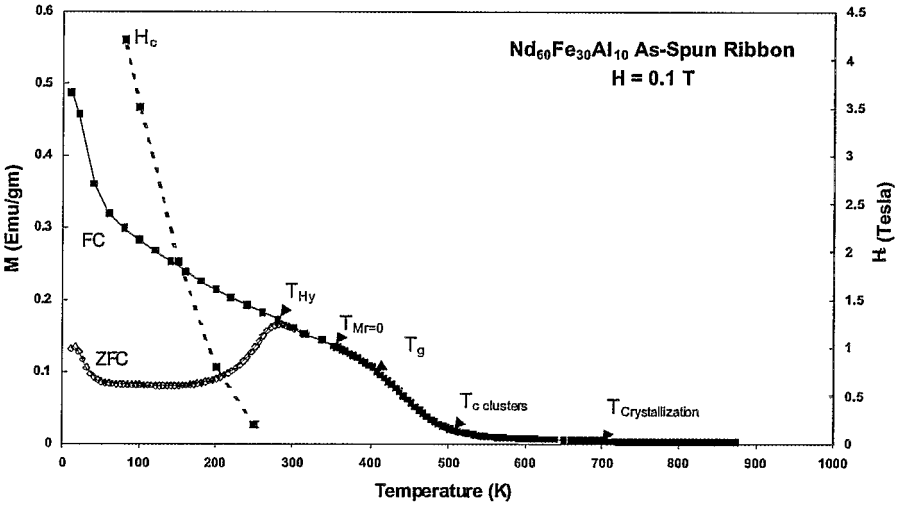

Figure 2: DC Magnetization versus temperature for $Nd_{60}Fe_{30}Al_{10}$.

complex picture. The M *vs.* H curves, which will be discussed in detail elsewhere[11], were not saturated in a field of 5 T at any temperature. Depending on temperature, 2 to 3 magnetic phases are required to describe the resultant hysteresis curves. In the temperature regime from 300 K > T > 400 K the materials exhibited zero remanent magnetization and the closed hysteresis loops can be fitted by assuming that the samples consist of superparamagnetic clusters and a paramagnetic matrix. As the temperature is lowered below T = 300 K, coercivity develops rapidly while below T = 50 K there is evidence for a second phase of lower coercivity. The onset of coercivity in the samples corresponds to the divergence of the ZFC and FC measurements. All five measured compositions exhibit similar behavior although the characteristic temperatures vary as a function of composition.

Figure 3 displays the thermoremanent magnetizations for all five compositions. Again there is evidence for the existence of two coercive phases. The low-temperature data is in agreement with the the results of the M *vs.* H data while data obtained near room temperature indicates that a non-zero coercivity persists to higher temperatures. As the thermoremanent magnetization is sensitive to very low values of the coercivity, this result points to a reasonably wide temperature region where the coercivity is non-zero but is less than ~10 mT. The data also demonstrate that the coercivity of the material disappears at a temperature that is approximately 70% of Curie temperature T_c of the system, which is 500 K (Figure 2). The compositional dependence of the thermoremanent magnetization curves is of particular interest. Even though the composition of the five samples varies roughly linearly in Al content, the spacing of the curves is far from linear. While the magnetization of the three samples in the middle of the composition range have very similar temperature dependencies, the low Al content sample is characterized by significantly higher magnetization while the highest Al content sample has significantly lower magnetization at any given temperature.

The thermoremanent magnetization reflects the thermal relaxation of the magnetization. However the time scale of the measurement is poorly defined since the relaxation observed is integrated over the entire time-temperature history following the field being set to zero. In order to qualitatively determine relaxation times it is necessary to perform AC susceptibility studies where the time scales are well defined. For a system of superparamagnetic particles that exhibit a single blocking temperature, the temperature dependence of the AC susceptibility as a function of frequency is given by the Casimir and Du Pre'[12] equations, which were originally developed for

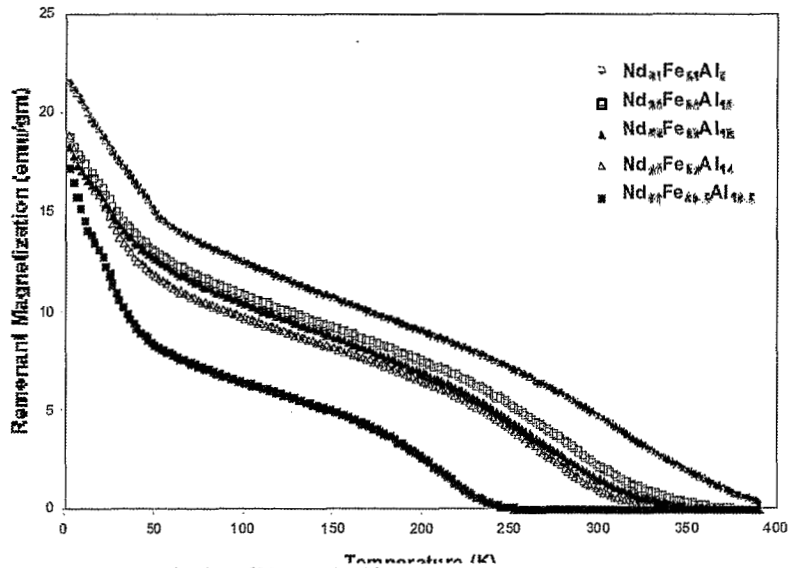

Figure 3: Thermoremanent magnetization of $Nd_{60-\delta}Fe3_{0-x}Al_{10+\delta+x}$.

the characterization of paramagnetic salts. When the measurement frequency is equal to the relaxation frequency of the magnetic moments there is a maximum in the AC loss term, χ". Thus the blocking temperature of a superparamagnet is equal to the peak temperature of the AC susceptibility loss χ" and not equal to the the AC susceptibility itself, χ'. The same argument applies to spin glass transitions. However the interactions between the moments greatly complicates the frequency dependence of the transition.

In Figure 4, the loss term of the frequency-dependent AC susceptibility χ" is shown as a function of temperature for the $Nd_{60}Fe_{30}Al_{10}$ composition. The clear frequency dependence of the AC loss term demonstrates that this signal is either a blocking temperature for an ensemble of superparamagnetic particles or is a spin-glass freezing temperature. While similar behavior is observed for Al contents in the alloys greater than 10 at%, the peak shapes for some compositions are quite broad. The peaks in both the AC susceptibility and AC loss signals for the Al = 8 at% ribbons are above the 400 K measurement limit of the SQUID magnetometer. As is shown in

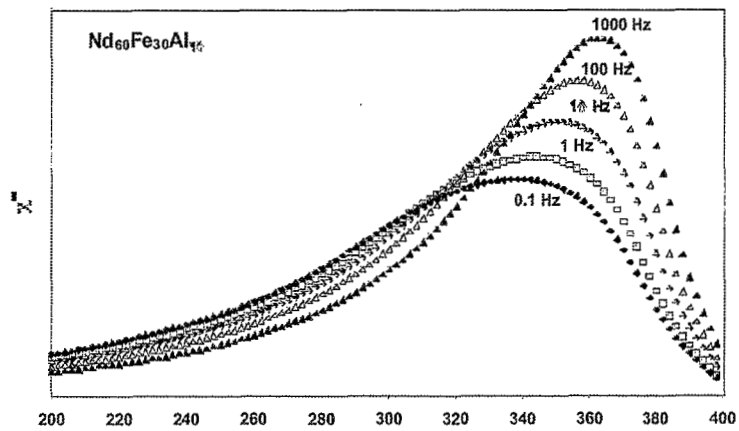

Figure 4: The AC loss term, χ", for $Nd_{60}Fe_{30}Al_{10}$ as a function of frequency.

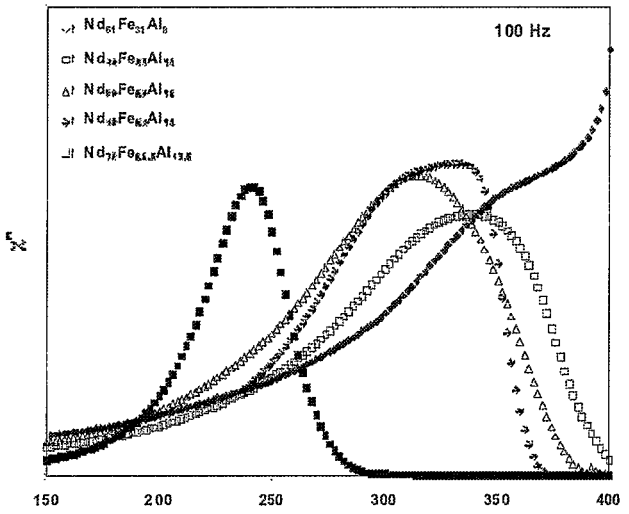

Figure 5: The AC loss term, χ", as a function of temperature for each of the five ribbon compositions.

Figure 5, where χ" at 100 Hz is plotted versus temperature for all five ribbon compositions the temperatures where χ" is a maximum follow the same trend as is observed in the thermoremanent magnetization.

5. Discussion

While the microstructural characterization clearly shows that these ribbons are truly nanocomposites, it provides limited information concerning the nature of the constituent nanophases. However a comparison of the magnetic properties as a function of temperature with the known properties of the phases present in the equilibrium phase diagram suggests some simple correlations can be made. The M *vs.* H data, the thermoremanent magnetization data and the AC susceptibility measurements make it clear that the deviation from Curie-Weiss behavior observed in the DC magnetization at T ~ 500 K for all compositions is associated with the existence of superparamagnetic clusters in the ribbons. These clusters are highly interacting, and thus it is appropriate to deem the nominally-amorphous samples as "cluster glasses". As will be shown in detail elsewhere the inability to saturate the magnetization in fields up to 5 T at all temperatures is attributed to a paramagnetic matrix. From the equilibrium Nd-Fe-Al phase diagram it is possible to speculate about the compositional nature of these superparamagnetic clusters. There are two ferromagnetic equilibrium phases in the Nd-Fe-Al phase diagram with a T_c of ~500 K. The crystallographically-complex μ-phase ($Nd_{37}Fe_{58}A_{l5}$) is reported to have a T_c= 500 K[13] while the T_C of ferromagnetic compound $Nd_2Fe_{17-x}Al_x$ ranges from 300 K to 500 K[14]. From the equilibrium phase diagram the $Nd_2Fe_{17-x}Al_x$ phase should not be present in any of the ribbon samples and the μ-phase should only be present in the ribbon containing 8 at% Al.. While none of the synthesized compositions fall in the primary solidification regions for these phases, the formation of clusters in the melt or during quenching is highly dependent on kinetic considerations. For the compositions of interest, the formation of such clusters can significantly lower the total energy of the system below that of the liquid, even though they do not represent the lowest energy state of the system.

From the DC magnetization and the thermoremanent magnetization data it is not possible to differentiate between thermal blocking of the superparamagnetic clusters and a spin glass transition. However for an ideal non-interacting collection of superparamagnetic clusters with a single blocking temperature T_B, Casimir and Du Pre'[12] showed that

$$\ln(\omega_m/\omega_0) = -\Delta/k_B T_{bl} \qquad \text{Eq. 1}$$

where ω_m is the measurement frequency and ω_0 (typically 10^8 to 10^{10}) is the attempt frequency for jumps over the anisotropy barrier, Δ. In a system with a distribution of blocking temperatures, a mean blocking temperature is measured which should also obey this equation. For a system obeying the Casimir – Du Pre' equation, a plot of $\ln(\omega_m)$ versus $1/k_B T_{bl}$ should be a straight line with slope Δ and intercept $\ln(\omega_0)$. While application of Eq. 1 to data obtained from samples of this study do yield straight lines, the values obtained for Δ and ω_0 are highly unphysical with $\omega_0 \sim 10^{100}$ and barrier heights Δ in the 10000 K range. While there are no successful simple models for the frequency dependence of spin glass transitions. Monte Carlo calculations for strongly interacting superparamagnetic particles predict a spin glass ordering temperature consistent with the current observations[15].

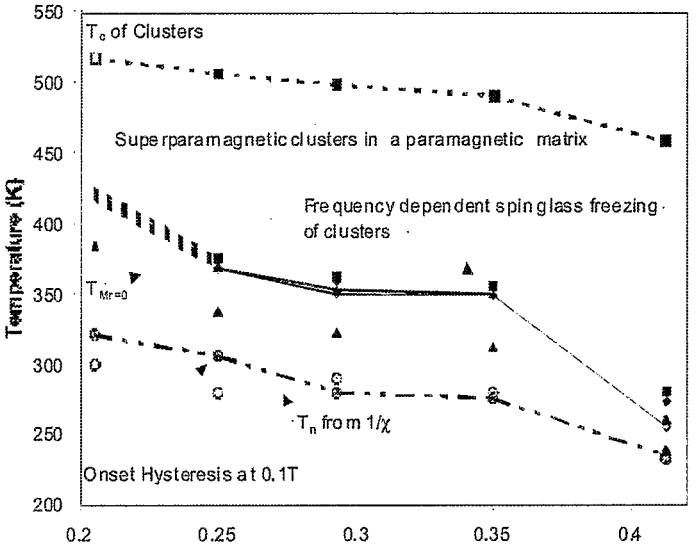

Figure 6: Magnetic phase diagram as a function of Al/(Al+Fe) ratio.

In Figure 6, the characteristic magnetic temperatures of the NdFeAl system are plotted as a function of Al content to provide a magnetic phase diagram. From the equilibrium phase diagram of Figure 1 it is apparent that the ribbon with 8 at% Al falls in the three- phase region Nd-δ-μ, while the 16.5 at% Al ribbon resides in the Nd- δ-Nd_3Al three-phase region. The samples with intermediate Al contents consist predominately of two-phase Nd-δ. Since the δ-phase is a peritectic phase in the primary solidification region of $Nd_2Fe_{17-x}Al_x$, the metastable extension of the liquidus line for the formation of $Nd_2Fe_{17-x}Al_x$ may be expected to extend into much of the phase regions where the δ-phase is formed. Thus for the ribbon containing 8 at% Al, clusters of Nd, δ, μ and $Nd_2Fe_{17-x}Al_x$ may reasonably be expected to exist in the system. For ribbons containing 16.5 at% Al, clusters of composition Nd, δ, Nd_3Al, and/or $Nd_2Fe_{17-x}Al_x$ can form, while

cluster compositions of Nd, δ, and $Nd_2Fe_{17-x}Al_x$ clusters are expected to form for ribbons of the intermediate Al content. Application of the lever law demonstrates that the ribbon with the 8 at% Al has a higher density of ferromagnetic clusters while the 16.5 at% Al ribbon has a relatively low concentration of such clusters. Within the Nd - δ two-phase region the cluster density is expected to be relatively constant. The cluster glass transition temperatures directly reflect the density of ferromagnetic clusters. Clusters consisting of Nd and the δ-phase are expected to be present in all compositions. The onset of large coercivities is concurrent with the Néel temperature of the δ phase. This result is consistent with calculations by Schulthess and Butler[16] which show that compensated antiferromagnetic-ferromagnetic interfaces produce extremely large uniaxial anisotropies. Finally it is interesting to note that while Nd with the double hexagonal close-packed structure has spins which order antiferromagnetically on the hexagonal sites at T = 19 K and on the cubic sites at T = 7.5 K, rapid quenching stabilizes the face-centered-cubic form of Nd which is ferromagnetic at T = 29 K[17]. Thus it is reasonable to associate the increase in the magnetization which is observed below T ≅ 50K (Fig. 2) with the ferromagnetic ordering of a Nd-rich matrix phase which surrounds the various clusters.

While the magnetic properties of melt-spun ribbons of $Nd_{60}Fe_{30-x}Al_{10+x}$ ($-2 \leq x \leq 6.5$) reflect a complex mixture of nanometric clusters, the existence of these clusters must play an important role in the bulk metallic glass formation as well as the collective magnetic properties. From the measured magnetic properties it appears that there are a large number of local atomic arrangements that approximate equilibrium crystal structures. These clusters are thought to significantly lower the free energy of the glass and decrease the driving force for further crystallization and are therefore instrumental in the solidification properties of the system.

Research performed under the auspices of the U.S. Dept. of Energy, Division of Materials Sciences, Office of Basic Energy Sciences. Ames Laboratory is operated by Iowa State University for the Department of Energy under Contract No. W-7405-ENG-82. Brookhaven Nation Laboratory is operated under contract No. DE-AC02-98CH10886.

[1] Akihisa Inoue, Tao Zhang, Wei Zhang and Akira Takeuchi, *Materials Trans, JIM* **37** (2) 99 (1996).
[2] Bing Chen Wei, Yong Zhang, Yan Xin Zhuang, De Qian Zhao, Ming Xiang Pan, Wei Hua Wang and Wen Rui Hu, *J. Appl. Phys.* **89** (6) 3529 (2001).
[3] H. Chiriac and N. Lupu, *J. Magn. Magn. Mater.* **196-197** (1999) 235-237.
[4] E. Callen, Y. J. Liu, and J. R. Cullen, *Phys. Rev. B.* **16** (1) (1977) 263 -270
[5] E. C. Stoner and E. P. Wohlfarth, *Philos Trans. R. Soc. Lond. A* **240** (1948) 599
[6] P. Gaunt, *Phys. Rev. B.* **19** (1) (1979) 521 -524
[7] A. S. O'Connor, L. H. Lewis, R. W. McCallum, K. W. Dennis, M. J. Kramer, D. T. Kim Anh, N. H. Dan, N. H. Luong and N. X. Phuc, Proceedings of the 16th International Workshop on Rare-Earth Magnets and Their Applications, Sendai, Japan (2000) H. Kaneko, M. Homma and M. Okada, eds.,. 475-482.
[8] M.J. Kramer, A. S. O'Connor, K. W. Dennis, R. W. McCallum, L. H. Lewis, L. D. Tung and N. P. Duong, *IEEE Trans. Magn.* **37** (4) 2497 (2001).
[9] N. H. Dan, V. H. Ky, N. X. Phuc, N. Chau, N. H. Luong, C. X. Huu, L. H. Lewis, R.W. McCallum, Proceedings of the MRS Spring 2001 Meeting, *in press*.
[10] R. W. McCallum et al to be published
[11] R. W. McCallum et al to be published
[12] H. B. G. Casimir and F. K. du Pre' *Physica's Grav.* **5** (1938) 507
[13] R. Politano, A. C. Neiva, H. R. Rechenberg and F. P. Missell, *J. Alloys and Comp.* **184** (1992) 121-129
[14] F. Weitzer, K. Hiebl and P. Rogl, *J. Appl. Phys.* **65** (12) 4963-4967 (1989).
[15] R. W. Chantrell, N. Walmsley, J. Gore, Maylin, M., *Phys. Rev. B*: (2001), **63**(2), 024410/1-024410/14.
[16] T. C.Schulthess, W. H. Butler, *Journal of Applied Physics* (1999), **85**(8, Pt. 2B) 5510-5515
[17] E. Bucher, C. W. Chu, J. P. Maita, K. Andres, A. S. Cooper, E. Buehler and K. Nassau, *Phys. Rev. Lett.* **22** (1969) 1260.